

Imaging through scattering layers using a near-infrared low-spatial-coherence fiber random laser

Anda Shi(史安达), Zeyu Wang(王泽宇), Chenxi Duan(段辰锡), Zhao Wang(王昭), and Weili Zhang(张伟利)

Citation: Chin. Phys. B, 2024, 33 (**10**): 104202. DOI: 10.1088/1674-1056/ad6420
Journal homepage: http://cpb.iphy.ac.cn; http://iopscience.iop.org/cpb

What follows is a list of articles you may be interested in

Principle of subtraction ghost imaging in scattering medium

Qin Fu(付芹), Yanfeng Bai(白艳锋), Wei Tan(谭威), Xianwei Huang(黄贤伟), Suqin Nan(南苏琴), and Xiquan Fu(傅喜泉)

Chin. Phys. B, 2023, 32 (**6**): 064203. DOI: 10.1088/1674-1056/acb202

Refocusing and locating effect of fluorescence scattering field

Jian-Gong Cui(崔建功), Ya-Xin Yu(余亚鑫), Xiao-Xia Chu(楚晓霞), Rong-Yu Zhao(赵荣宇), Min Zhu(祝敏), Fan Meng(孟凡), and Wen-Dong Zhang(张文栋)

Chin. Phys. B, 2021, 30 (**12**): 124210. DOI: 10.1088/1674-1056/ac2804

Controlling the light wavefront through a scattering medium based on direct digital frequency synthesis technology

Yuan Yuan(袁园), Min-Yuan Sun(孙敏远), Yong Bi(毕勇), Wei-Nan Gao(高伟男), Shuo Zhang(张硕), and Wen-Ping Zhang(张文平)

Chin. Phys. B, 2021, 30 (**1**): 014209. DOI: 10.1088/1674-1056/abb665

Memory effect evaluation based on transmission matrix calculation

Ming Li(李明), Long-Jie Fang(方龙杰), Lin Pang(庞霖)

Chin. Phys. B, 2019, 28 (**7**): 074207. DOI: 10.1088/1674-1056/28/7/074207

Lensless ghost imaging through the strongly scattering medium

Zhe Yang(杨哲), Lianjie Zhao(赵连洁), Xueliang Zhao(赵学亮), Wei Qin(秦伟), Junlin Li(李俊林)

Chin. Phys. B, 2016, 25 (**2**): 024202. DOI: 10.1088/1674-1056/25/2/024202

Imaging through scattering layers using a near-infrared low-spatial-coherence fiber random laser

Anda Shi(史安达)[1,†], Zeyu Wang(王泽宇)[1,†], Chenxi Duan(段辰锡)[2,†], Zhao Wang(王昭)[1,‡], and Weili Zhang(张伟利)[1]

[1] *School of Information and Communication Engineering, University of Electronic Science & Technology of China, Chengdu* 611731, *China*
[2] *Yingcai Honors College, University of Electronic Science & Technology of China, Chengdu* 611731, *China*

(Received 13 May 2024; revised manuscript received 9 July 2024; accepted manuscript online 17 July 2024)

Optical memory effect-based speckle-correlated technology has been developed for reconstructing hidden objects from disordered speckle patterns, achieving imaging through scattering layers. However, the lighting efficiency and field of view of existing speckle-correlated imaging systems are limited. Here, a near-infrared low spatial coherence fiber random laser illumination method is proposed to address the above limitations. Through the utilization of random Rayleigh scattering within dispersion-shifted fibers to provide feedback, coupled with stimulated Raman scattering for amplification, a near-infrared fiber random laser exhibiting a high spectral density and extremely low spatial coherence is generated. Based on the designed fiber random laser, speckle-correlated imaging through scattering layers is achieved, with high lighting efficiency and a large imaging field of view. This work improves the performance of speckle-correlated imaging and enriches the research on imaging through scattering medium.

Keywords: fiber random laser, speckle-correlated imaging, scattering medium, spatial coherence

PACS: 42.25.Dd, 42.30.–d, 42.55.Ye **DOI:** 10.1088/1674-1056/ad6420

1. Introduction

Imaging is one of the important ways for humans to obtain information, playing a crucial role in promoting cognition, information exchange, and decision-making. With the advancement of science and technology, human beings have greatly improved their ability to obtain information through imaging. For example, the emergence of microscopes allows us to see more finely, and the emergence of telescopes enables us to see further. However, when signal light passes through strong scattering media (such as biological tissues, clouds, fog, etc.), random modulation from scattering media will result in spatially disordered speckle patterns, and the interested object information is submerged in noise. In recent years, many new methods and technologies have been proposed for recovering useful information from disordered speckle patterns, such as wavefront shaping,[1–3] transmission matrix measurement,[4–6] deep learning,[7–10] speckle-correlated imaging,[11–16] and so on.

Speckle-correlated imaging based on the optical memory effect (OME) has advantages such as strong generalization, non-invasive, fast imaging speed, and simple device, which has been widely studied, from scanning imaging to single-shot imaging, from two-dimensional imaging to three-dimensional imaging, from monochromatic imaging to color imaging, and then to multi-spectral imaging.[11,12,14,17,18] At present, the illumination source of speckle-correlated imaging systems mainly uses narrowband spatially incoherent light, which is usually generated in two ways: one is a narrow linewidth laser passing through fast-rotating ground glass,[12,19,20] and the other is a narrowband filtered light-emitting diode (LED)/amplified spontaneous emission (ASE) source.[21,22] However, due to the non-directional scattering of ground glass, and the specified wavelength selection of narrowband filters, the lighting efficiency of these two methods is relatively low.

On the other hand, the OME is mainly dominated by ballistic photons and single-scattering photons.[23] For most biological tissues, the intensity of light scattering is inversely proportional to λ^{α} (λ is the wavelength of the signal light, and $\alpha < 3$).[24] Therefore, compared with visible light, near-infrared light has more ballistic photons and single-scattering photons after passing through the scattering medium, theoretically resulting in a larger range of OME and a larger imaging field of view (FOV). However, in existing OME-based speckle-correlated imaging systems, the wavelength of the illumination source mainly focuses on visible light, and there is relatively little imaging under near-infrared illumination.

In this work, a near-infrared low spatial coherence fiber random laser illumination method is proposed and validated to improve the FOV and lighting efficiency of speckle-correlated imaging systems. Through the utilization of random Rayleigh scattering within dispersion-shifted fibers to provide feedback, coupled with stimulated Raman scattering for amplification, a near-infrared fiber random laser with high spectral density

[†]These authors contributed equally to this work.
[‡]Corresponding author. E-mail: z_wanguestc@outlook.com

© 2024 Chinese Physical Society and IOP Publishing Ltd

(3-dB spectral bandwidth of 2.4 nm) and extremely low spatial coherence (speckle contrast of 0.048) is generated. Then, based on the illumination of the designed fiber random laser, high lighting efficiency speckle-correlated imaging through scattering media is achieved. Moreover, compared to visible light illumination at 635 nm, the proposed near-infrared illumination method improves the FOV of the speckle-correlated imaging system by approximately 1.72 times. The proposed illumination method can be potentially applied to biological tissue imaging, light-scattering imaging, and other spatially incoherent illumination imaging.

2. Near-infrared low spatial coherence fiber random laser

The OME shows that the point spread function (PSF) of speckle-correlated imaging systems has a linear translation-invariant property within a certain range of FOV. Therefore, under spatially incoherent illumination, the speckle patterns (donated as I) formed by an object passing through a scattering medium can be mathematically described as a convolution of the object (donated as O) and PSF[12,19,25]

$$I = O * \mathrm{PSF}, \tag{1}$$

where $*$ represents the convolution operation. Due to the decrease of speckle contrast with the increase of spectral bandwidth of incoherent illumination sources, to preserve effective information, narrowband spatially incoherent light is usually chosen as the illumination source of speckle-correlated imaging systems. In this work, different from previous narrowband spatial incoherent illumination ways, where usually using either a narrow linewidth laser passing through a fast-rotating ground glass or a narrowband filtered ASE/LED, a near-infrared low spatial coherence fiber random laser illumination method is proposed with higher lighting efficiency and larger FOV.

Raman fiber random laser is a new type of laser source with advantages such as flexible working wavelength, high power, and high stability.[26–28] Making full use of the advantages of Raman fiber random laser, the near-infrared low spatial coherence fiber random laser (LSCFRL) is first designed, as shown in Fig. 1(a). The pump source is a Raman fiber laser with a central wavelength of 1365 nm. To achieve low threshold and high-efficiency random laser lasing, a 6-km long dispersion-shifted fiber (DSF) with a high Raman scattering coefficient is selected as the Raman fiber serving as the gain medium. The 1365-nm Raman laser is coupled into the DSF via a wavelength division multiplexer. Subsequently, backward Rayleigh scattering within the DSF provides intensity feedback, while stimulated Raman scattering provides optical amplification, forming the fiber random laser. A 9:1 coupler is used to guide the output of the fiber random laser. Among them, 90% of the port of the coupler is connected to a power meter (Newport 843-R) to measure the power of fiber random laser, and 10% of the port is connected to an optical spectrum analyzer (MS9710C) to analyze the spectral change.

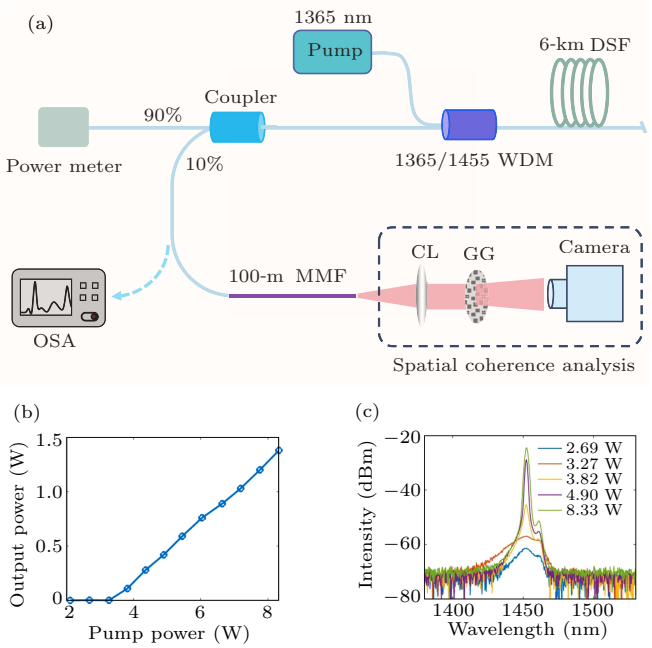


Fig. 1. The design of near-infrared LSCFRL and its output characteristics. (a) Experimental setup of the LSCFRL. (b) The power output characteristic of the LSCFRL. (c) Spectral characteristics of the LSCFRL. DSF: dispersion-shifted fiber, OSA: optical spectrum analyzer, MMF: multimode fiber, CL: collimated lens, GG: ground glass.

The power output characteristic of the fiber random laser is shown in Fig. 1(b). In the beginning, since the pump power has not yet reached the threshold of stimulated Raman scattering, spontaneous Raman scattering is dominant. The light-to-light conversion efficiency of spontaneous Raman scattering is low (only 10^{-6} of the incident light energy is converted to Stokes light), so the output power is small. When the pump power exceeds 3.27 W, the threshold condition of stimulated Raman scattering is reached, and the power of the fiber random laser increases greatly. Under the mechanism of stimulated Raman scattering, the light-to-light conversion efficiency is greatly improved, and the power of the fiber random laser increases linearly with the increase of pump power. When the pump power is 8.33 W, the output power of the fiber random laser reaches 1.38 W.

The spectral characteristic of the fiber random laser is shown in Fig. 1(c). In the beginning, spontaneous Raman scattering is dominant. When the pump power is 2.69 W, the central wavelength of spontaneous Raman radiation is 1452 nm, with a 3-dB spectral bandwidth of approximately 13.8 nm. If the threshold of stimulated Raman scattering is reached (i.e., the pump power is greater than 3.27 W), mode (longitudinal mode) competition will lead to a sharp decrease in the 3-dB spectral bandwidth of fiber random lasers. When the pump

power is 3.82 W, the central wavelength of stimulated Raman radiation is 1452 nm and the bandwidth is approximately 2.4 nm. As the pump power increased from 3.82 W to 8.33 W, the central wavelength of the fiber random laser remained stable at 1452 nm, and the 3-dB bandwidth remained almost unchanged at 2.4 nm. Therefore, the designed fiber random laser has high stability and spectral density.

In the imaging experiment based on near-infrared fiber random laser, the OSA is replaced by a 100-m long step refractive index multimode fiber (MMF, core/cladding diameter: 105 μm/125 μm, NA 0.22). The MMF is connected to the 10% ports of the coupler, which is used to reduce the spatial coherence of the laser source. Due to the existence of numerous modes (transverse mode) in MMF, when the transmission delay of different modes is greater than the coherence time of the laser source, diverse modes will be incoherently intensity superimposed forming a spatially incoherent illumination source.[28,29] Therefore, different from the narrow linewidth laser transmission in MMF, where diverse modes are coherently superimposed, distinct speckle patterns will be formed at the output end of the MMF. The intensity distribution of the random laser from MMF exhibits a smooth transition characteristic, without speckle grains, as shown in Fig. 2(a1).

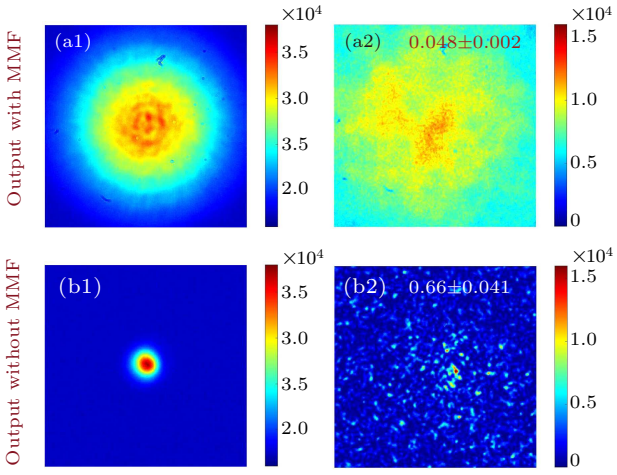


Fig. 2. Spatial coherence of the designed fiber random laser. (a1) Mode profile of fiber random laser at the output end of the MMF, (a2) speckle patterns corresponding to panel (a1). (b1) Mode profile of fiber random laser at the output end of the single mode fiber, (b2) speckle patterns corresponding to panel (b1). MMF: multimode fiber.

The speckle contrast of speckle patterns decreases with the decrease of spatial coherence, which is used to quantitatively analyze the spatial coherence of laser sources.[27,30] Thus, to analyze the spatial coherence of the designed fiber random laser, a piece of 400-grit ground glass (Zolix, grit 400) is used to scatter the laser source, and then a near-infrared camera (Xenics, Bobcat-640 Gige, resolution of 512×640, pixel pitch of 20 μm) is used to capture the speckle patterns. Under the guidance of MMF, figure 2(a2) shows the speckle patterns formed by the fiber random laser passing through the scattering medium, exhibiting a relatively uniform intensity distribution. Furthermore, calculate the speckle contrast (C):

$$C = \frac{\sigma_I}{\langle I \rangle}, \tag{2}$$

where σ_I is the standard deviation of speckle patterns, and $\langle I \rangle$ is the average intensity of speckle patterns. To reduce data fluctuations and improve the reliability of data calculations, the scattering medium is shifted to 10 different positions, and the corresponding 10 sets of experimental data are measured. Subsequently, the statistical mean and standard deviation of I are calculated. When the fiber random laser (FRL) guided by MMF, the speckle patterns formed by FRL passing through scattering medium has a speckle contrast as low as 0.048±0.002, which is close to the perception threshold of the human eye (0.04), indicating that the designed laser source has a low spatial coherence.

In contrast, the spatial coherence of fiber random lasers is also analyzed without the guidance of MMF. Figure 2(b1) shows the mode profile of the fiber random laser, exhibiting the classical Gaussian intensity distribution characteristic, which corresponds to the characteristic of the fundamental mode of single-mode fiber. Under the guidance of single-mode fiber, figure 2(b2) shows the speckle patterns formed by the fiber random laser passing through the scattering medium, with a speckle contrast of 0.66±0.041, indicating that the laser source has a high spatial coherence.

Based on the above analyses, the designed fiber random laser guided by MMF has a low spatial coherence, so it can be used for imaging of spatially incoherent illumination, such as speckle-correlated imaging, microscopic imaging, and so on.

3. Optical memory effect-based speckle-correlated imaging through scattering layers

Under the illumination of the homemade near-infrared LSCFRL, optical memory effect-based speckle-correlated imaging through scattering layers is realized. The experimental setup is shown in Fig. 3(a). The output of the fiber random laser is collimated by a convex lens (focal length of 6.2 mm), and then irradiates on the digital micro-mirror device (DMD, DLPLCR65NEVM, Texas Instruments). DMD can load any two-dimensional pattern serving as the imaging object. In the experiment, the handwritten digit "7", five symmetrically distributed points, and the Chinese character "Tian" are loaded onto the DMD, as shown in the bottom left corner of Figs. 4(b1)–4(b3). Besides, by loading a point (54 μm×54 μm) onto the DMD, the PSF of the scattering imaging system is measured as shown in Fig. 4(a). To validate the speckle-correlated imaging, a piece of ground glass (Zolix, grit 400) is placed between the object (i.e., DMD) and the camera serving as scattering media, scattering signal light from the object. The distance from the ground glass to the DMD and camera is 12 cm and 4 cm, respectively. The signal light from DMD forms speckle patterns after passing through the scattering medium, which is collected using a near-infrared

camera (Xenics, Bobcat-640 Gige), as shown in Figs. 4(b1)–4(b3). The camera exposure time is dynamically adjusted according to the power of the near-infrared fiber laser and the sparsity of the object.

Based on Eq. (1), under the precondition of obtaining the PSF of the scattering imaging system, the deconvolution algorithm can be used to reconstruct objects from speckle patterns.[14,16,31] The speckle-correlated imaging under Richardson–Lucy deconvolution reconstruction is shown in Figs. 4(c1)–4(c3), where the handwritten digit "7", five symmetrically distributed points, and the Chinese character "Tian" are reconstructed with a high contrast and signal-to-noise ratio. Thus, the homemade near-infrared LSCFRL can serve as the illumination source of speckle-correlated imaging systems.

In contrast to conventional illumination ways utilized in speckle-correlated imaging systems, such as narrow linewidth laser passes through fast-rotating ground glass or narrow-band filtered LED/ASE configurations, the proposed near-infrared LSCFRL illumination approach offers superior lighting efficiency. This is attributed to its high spectral density (3-dB spectral bandwidth of 2.4 nm) and extremely low spatial coherence (speckle contrast of 0.048), thereby obviating the non-directional scattering introduced by ground glass and the energy losses introduced by narrow-band filters. The qualitative evaluation of lighting efficiency is shown in Appendix B. Moreover, in speckle-correlated imaging systems, the range of OME increases with the increase of signal light wavelength. Therefore, under the illumination of the proposed near-infrared LSCFRL, the imaging system is expected to have a larger FOV.

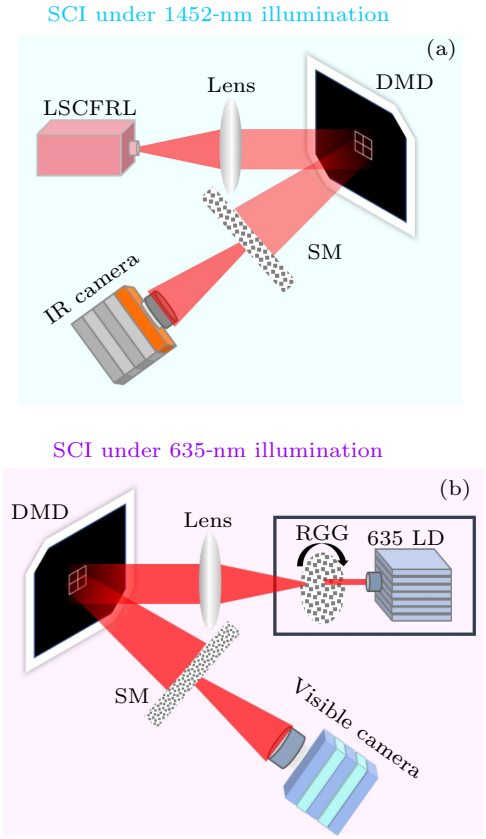


Fig. 3. Optical memory effect-based speckle-correlated imaging through scattering medium under the illumination of LSCFRL (a) and 635-nm illumination (b). SCI: speckle-correlated imaging, DMD: digital micro-mirror device, SM: scattering medium, IR camera: near-infrared camera, LD: laser diode.

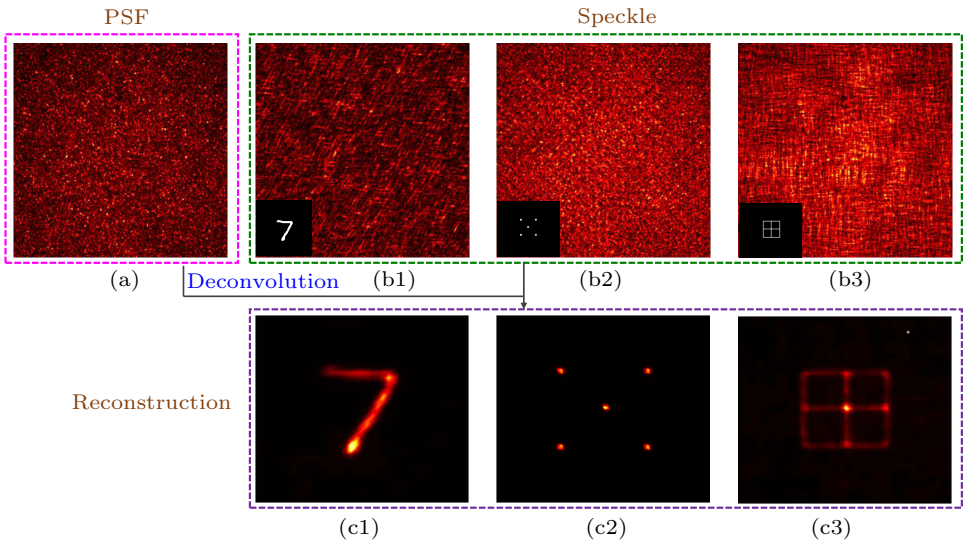


Fig. 4. Experimental results of speckle-correlated imaging under near-infrared fiber random laser illumination. (a) PSF of scattering imaging system, (b1)–(b3) speckle patterns formed by the handwritten digit "7", five symmetrically distributed points, and Chinese character "Tian" passing through the scattering medium, where the bottom left corner shows the ground value of the hidden objects, (c1)–(c3) Richardson–Lucy deconvolution reconstruction image.

To verify that speckle-correlated imaging systems under near-infrared illumination have a larger FOV, imaging is compared under the illumination of two wavelengths, 635 nm and 1452 nm. Except for the differences in illumination source and camera, the experimental setup of speckle-correlated imaging under two wavelengths of illumination is the same, as shown in Fig. 3. Among them, for speckle-correlated imaging system under 635-nm illumination (shown in Fig. 3(b)): to meet

the requirements of narrowband spatial incoherent illumination, the output of the 635-nm laser diode (FODL-43A-635-1) is passed through a fast-rotating ground glass; a visible camera (Andor Zyla 5.5, resolution of 2160×2560, pixel pitch of 6.5 μm) is used to collect speckle patterns formed by the objects passing through scattering medium.

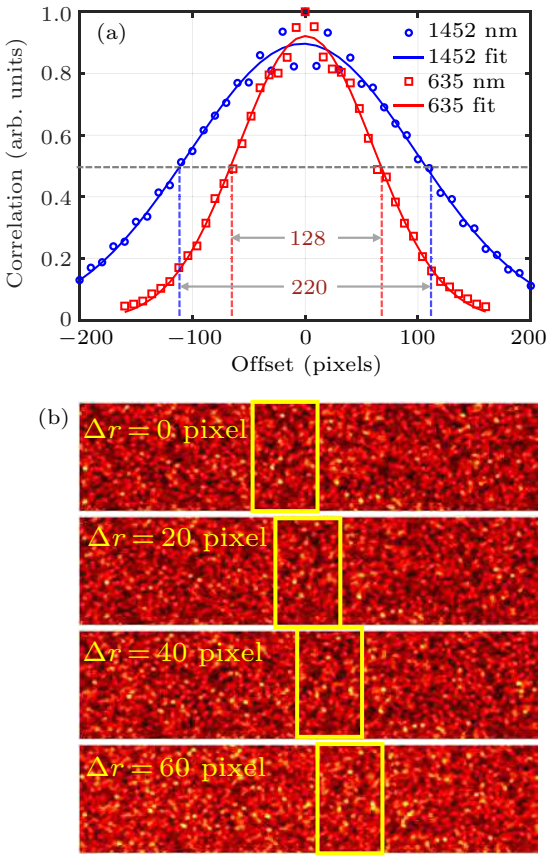


Fig. 5. Optical memory effect range of speckle-correlated imaging systems under illumination of 635 nm and 1452 nm. (a) The variation curve of $C(\Delta r)$. (b) The speckle patterns shift with the translation of the point (i.e., optical memory effect), and Δr in the figure represents the translation distance of the point.

Firstly, the range of OME under illumination of two wavelengths is compared. The range of optical memory effect range is decided by the scattering strength of scattering medium, the wavelength of the lighting source, and the object distance, which is independent of other parameters. The experimental setup for measuring the range of OME is shown in Fig. 3. A 5×5 point (54 μm×54 μm) is loaded on DMD, and the corresponding speckle patterns formed by passing through the scattering medium is labeled S_{r0}. Then, the point is translated along the x axis of the DMD in steps of 5 pixels (54 μm), and the corresponding speckle patterns is labeled as S_{ri}. Under the near-infrared illumination at 1452 nm, the S_{ri} at different translation distances is shown in Fig. 5(b), where the speckle patterns S_{ri} shifts with the translation of the point, indicating a high translation correlation between the speckle patterns, which is consistent with the essence of OME. The normalized cross-correlation between S_{ri} and S_{r0} is calculated, and the maximum (donated as $C(\Delta r)$) is extracted. Define the full width at half maximum (FWHM) of $C(\Delta r)$) as the range of OME. The numerical simulation is shown in Appendix A.

Under near-infrared illumination at 1452 nm, the correlation coefficient curve $C(\Delta r)$ is shown in the blue circle in Fig. 5(a), where the solid blue line represents Gaussian fitting with an FWHM of approximately 220 DMD pixels (i.e., 2376 μm). Thus, under near-infrared illumination at 1452 nm, the FOV of the speckle-correlated imaging system is 2376 μm. As a comparison, the correlation coefficient curve $C(\Delta r)$ of 635-nm illumination is shown in the red circle in Fig. 5(a), where the solid red line represents Gaussian fitting with an FWHM of approximately 128 DMD pixels (i.e., 1382.4 μm). Therefore, the range of OME under 1452-nm near-infrared illumination is larger, about 1.72 times that under 635-nm illumination.

Under the same experimental conditions, the speckle-correlated imaging system illuminated by near-infrared light has a larger range of OME. Thus, it can be expected that compared to visible light, near-infrared illumination has a larger FOV and can image larger objects. The range of FOV of the speckle-correlated imaging system under the illumination of two wavelengths is compared, as shown in Fig. 6. The first row in Fig. 6 is the object loaded on the DMD (the Chinese character "Tian"), with sizes of 90×90, 120×120, 150×150, 180×180, and 210×210 DMD pixels, located at the center of the DMD. Firstly, by loading a 5×5 point at the center of the DMD, the PSF of the scattering imaging system is measured. After obtaining speckle patterns formed by objects of different sizes passing through scattering media, the Richardson–Lucy deconvolution operation between speckle patterns and PSF is used to reconstruct the objects.

The Richardson–Lucy deconvolution reconstruction image under 1452-nm near-infrared illumination is shown in the second row of Fig. 6, where the white dashed box represents the range of OME. It is discernible that, for object sizes $\leq 180 \times 180$ DMD pixels, the object is within the range of OME, so the Chinese character "Tian" can be fully reconstructed; When the object sizes is 210×210 DMD pixels, the distance between the four corners and the center of the Chinese character "Tian" is greater than 220 pixels, which is outside the range of OME, resulting in a decrease in the signal-to-noise ratio of the reconstructed image. In contrast, the reconstructed image under 635-nm illumination is shown in the third row of Fig. 6. For object sizes $\geq 120 \times 120$ DMD pixels, the edge part of the objects is no longer within the range of OME, resulting in the Chinese character "Tian" cannot be fully reconstructed; When object size is 180×180 or 210×210 DMD pixels, only the cross line in the middle of the Chinese character "Tian" can be reconstructed.

Based on the above analyses, compared with 635-nm visible light illumination, the speckle-correlated imaging system under 1452-nm near-infrared light illumination can image larger objects and has a larger imaging FOV.

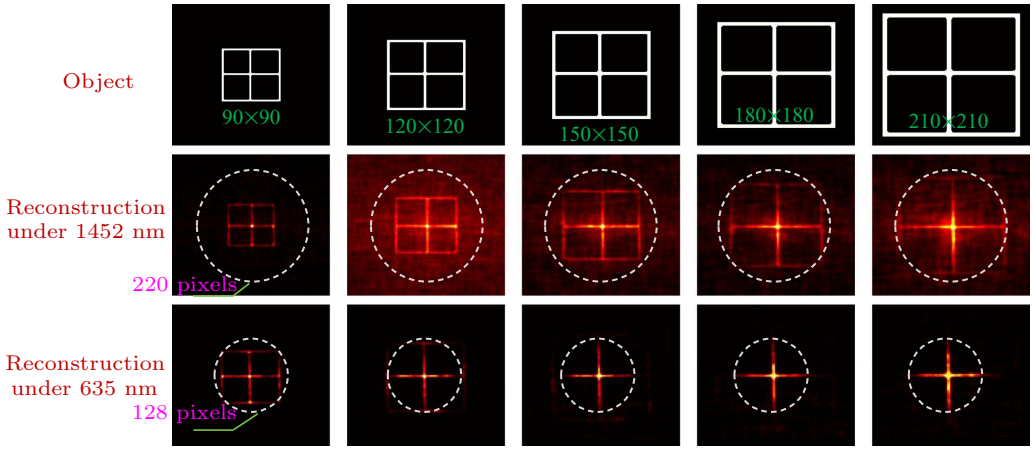


Fig. 6. Comparisons of the field of view of speckle-correlated imaging under illumination at two wavelengths of 635 nm and 1452 nm. The first row is the object loaded on the DMD. The second row shows the reconstructed image under 1452-nm illumination. The third row shows the reconstructed image under 635-nm illumination.

4. Conclusion

In the present investigation, a 1452-nm near-infrared fiber random laser illumination method is proposed with high spectral density (3-dB spectral bandwidth of 2.4 nm) and extremely low spatial coherence (speckle contrast of 0.048). Based on the illumination of the near-infrared fiber random laser, the speckle-correlated imaging through scattering layers is realized with a high lighting efficiency. Compared to 635-nm visible light illumination, the range of the optical memory effect under 1452-nm fiber random laser illumination has increased by 1.72 times.

Moreover, the Richardson–Lucy deconvolution reconstruction image also indicates that the speckle-correlated imaging system under 1452-nm fiber random laser illumination can image larger objects. The proposed illumination method can be potentially applied to biological tissue imaging, light-scattering imaging, and other spatially incoherent illumination imaging.

Appendix A: Numerical simulation of OME

Firstly, the PSF of scattering imaging system is considered, i.e., a point (50 μm×50 μm) propagating from the object plane to the scattering medium plane, and then to the image plane, as shown in Fig. A1(a). The propagation process can be described by Fresnel diffraction, as expressed as

$$\mathrm{PSF} = \left| \iint \exp\left(\frac{\mathrm{i}k}{2u}(x_\mathrm{s}^2 + y_\mathrm{s}^2)\right) T(x_\mathrm{s}, y_\mathrm{s}) \times \exp\left(\frac{\mathrm{i}k}{2v}[(x_\mathrm{I} - x_\mathrm{s})^2 + (y_\mathrm{I} - y_\mathrm{s})^2]\right) \mathrm{d}x_\mathrm{s}\,\mathrm{d}y_\mathrm{s} \right|^2, \quad \text{(A1)}$$

where the subscripts s and I denote the plane of scattering medium and image, respectively; u and v denotes the object distance (the distance from the object plane to the scattering medium plane, 5 cm) and the image distance (the distance from the scattering medium plane to the image plane, 10 cm), respectively, T corresponds to the random phase induced by scattering medium. The scattering medium is numerical generated with a correlation length 30 μm.

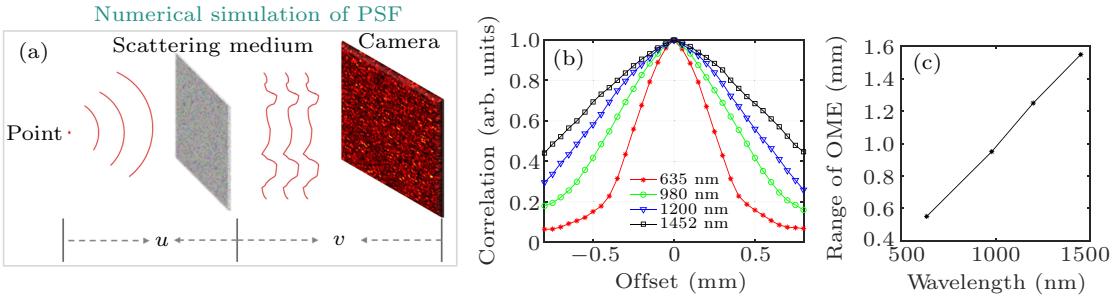


Fig. A1. The numerical simulation of PSF: (a) model of numerical simulation, (b) the correlation coefficient between PSFs under illumination of different wavelengths, (c) the range of OME for different wavelengths.

According to Eq. (A1), under illumination of different wavelengths, when the point is shifted to different spatial positions, the corresponding PSF is captured. Then, the correlation coefficient between PSFs under illumination of different wavelengths is calculated, as shown in Fig. A1(b). Define the full width at half maxima (FWHM) of the curve of correlation coefficient as the range of OME. Under illumination of 635 nm, 980 nm, 1200 nm, and 1452 nm, the range of OME of the

scattering imaging system are 0.55 mm, 0.95 mm, 1.25 mm, and 1.55 mm, respectively. Moreover, the curve of the range of OME changing with wavelength is plotted, as shown in Fig. A1(c). It can be seen that as the wavelength increases, the range of OME approximately linearly increases, which consists with the Ori's opinion (i.e., $\Delta\theta_{\mathrm{FOV}} \approx \lambda/(\pi l)$).[12]

Appendix B: Qualitative evaluation of lighting efficiency

In this work, a near-infrared LSCFRL illumination approach is proposed for speckle correlated imaging, which has larger field-of-view and higher lighting efficiency. To qualitatively evaluate the lighting efficiency, the proposed illumination method (i.e., the FRL guided by MMF, as shown in Fig. B1(a1)) and the traditional illumination way (i.e., a piece of fast-rotating ground glass is used to lower the spatial coherence of laser, as shown in Fig. B1(b1)) are compared. Except for the different lighting modules, the other experimental conditions are the same in Figs. B1(a1) and B1(b1), e.g., the power of the light source, the exposure time of the camera, etc. The speckle patterns captured by a near-infrared camera for the proposed illumination method and the traditional illumination way are shown in Figs. B1(a2) and B1(b2), respectively. Due to the non-directional scattering and insertion loss introduced by ground glass, the intensity of Fig. B1(b2) is obviously smaller compared to the intensity of Fig. B1(a2). To qualitatively evaluate the lighting efficiency, the average intensity of Figs. B1(a2) and B1(b2) are calculated, as shown in the white font in Figs. B1(a2) and B1(b2). For the former, the average intensity is 2.52×10^4; for the latter, the average intensity is 1.85×10^4. Therefore, compared to the traditional illumination way, the lighting efficiency of proposed illumination method has increased by 36%.

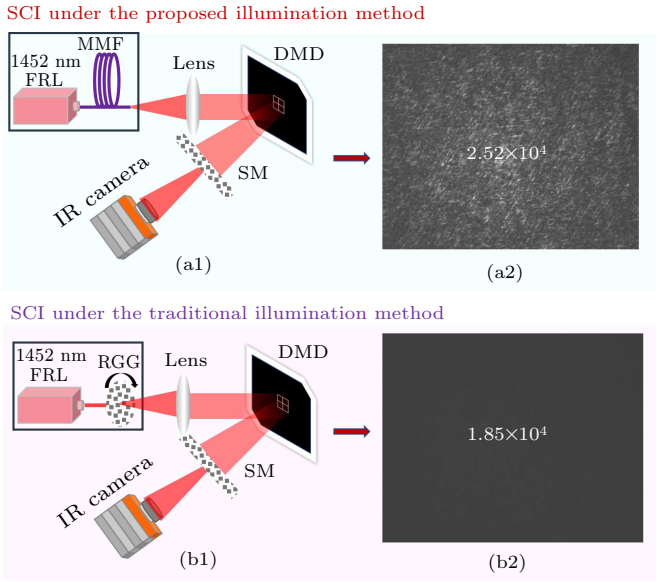


Fig. B1. Qualitative evaluation of lighting efficiency. (a1)/(b1) Speckle-correlated imaging using the proposed illumination method/traditional illumination way. (a2)/(b2) Speckle patterns corresponding to panels (a1)/(b1). SCI: speckle-correlated imaging, MMF: multimode fiber, DMD: digital micromirror device, SM, scattering medium, IR camera: near-infrared camera, RGG: fast-rotating ground glass.

Acknowledgements

Project supported by the National Natural Science Foundation of China (Grant Nos. 62375040 and 11974071) and the Sichuan Science and Technology Program (Grant Nos. 2022ZYD0108 and 2023JDRC0030).

References

[1] Yu Z, Li H, Zhong T, Park J H, Cheng S, Woo CM, Zhao Q, Yao J, Zhou Y, Huang X, Pang W, Yoon H, Shen Y, Liu H, Zheng Y, Park Y, Wang L V and Lai P 2022 *The Innovation* **3** 100292
[2] Yang J, He Q, Liu L, Qu Y, Shao R, Song B and Zhao Y 2021 *Light Sci. Appl.* **10** 149
[3] Woo C M, Zhao Q, Zhong T, Li H, Yu Z and Lai P 2022 *APL Photon.* **7** 046109
[4] Popoff S M, Lerosey G, Carminati R, Fink M, Boccara A C and Gigan S 2010 *Phys. Rev. Lett.* **104** 100601
[5] Lee K and Park Y 2016 *Nat. Commun.* **7** 13359
[6] Ma R, Luo K H, Pokharel S, Wang Z, Korotkova O, He J S, Zhang W L, Fan D Y, Gomes A S L and Liu J 2024 *Optica* **11** 595
[7] Li S, Deng M, Lee J, Sinha A and Barbastathis G 2018 *Optica* **7** 803
[8] Li Y, Xue Y and Tian L 2018 *Optica* **5** 1181
[9] Lyu M, Wang H, Li G, Zheng S and Situ G 2019 *Adv. Photon.* **1** 036002
[10] Zhu S, Guo E, Gu J, Bai L F and Hang J 2021 *Photon. Res.* **9** B220
[11] Bertolotti J, Van Putten E G, Blum C, Lagendijk A, Vos W L and Mosk A P 2012 *Nature* **491** 232
[12] Katz O, Heidmann P, Fink M and Gigan S 2014 *Nat. Photon.* **8** 784
[13] Ma R, Wang Z, Wang W Y, Zhang Y, Liu J, Zhang W L, Gomes A S L and Fan D Y 2021 *Opt. Lasers Eng.* **141** 106567
[14] Sahoo S K, Tang D and Dang C 2017 *Optica* **4** 1209
[15] Zhu L, Soldevila F, Moretti C, d'Arco A, Boniface A, Shao X, De Aguiar H B and Gigan S 2022 *Nat. Commun.* **13** 1447
[16] Wang D, Sahoo S K, Zhu X W, Adamo G and Dang C 2021 *Nat. Commun.* **1** 3150
[17] Horisaki R, Okamoto Y and Tanida J S 2019 *Opt. Lett.* **44** 4032
[18] Li X, Greenberg J A and Gehm M E 2019 *Optica* **6** 864
[19] Wu T, Katz O, Shao X and Gigan S 2016 *Opt. Lett.* **41** 5003
[20] Lu D, Liao M, He W, Giancarlo P, Wolfgang O and Peng X 2020 *Opt. Laser Eng.* **124** 105815
[21] Xu X, Xie X, Thendiyammal A, Zhuang H, Xie J, Liu Y, Zhou J and Allard P M 2018 *Opt. Express* **26** 15073
[22] Wu T, Dong J, Shao X and Gigan S 2017 *Opt. Express* **25** 27182
[23] Liu H, Liu Z, Chen M, Han S and Wang L V 2019 *Photon. Res.* **7** 1323
[24] Jacques S L 2013 *Phys. Med. Biol.* **58** R37
[25] Ma R, Wang Z, Zhang H H, Zhang W L and Rao Y J 2020 *Opt. Lett.* **45** 3816
[26] Yang Q, Li Y, Zou H, Mei J, Xu E M and Zhang Z X 2024 *Chin. Phys. B* **33** 024206
[27] Wang S, Zhang W, Yang N, Ma R, Zhang Y, Wang Z, Zhang J and Rao Y 2021 *Ann. Phys.* **533** 2100390
[28] Ma R, Rao Y J, Zhang W L and Hu B 2018 *IEEE J. Sel. Top. Quant.* **25** 1
[29] Redding B, Ahmadi P, Mokan V, Seifert M, Choma M A and Cao H 2015 *Opt. Lett.* **40** 4607
[30] Redding B, Choma M A and Cao H 2012 *Nat. Photon.* **6** 355
[31] Wang Z, Ma R, Liu J, He J and Zhang W 2023 *Appl. Phys. Lett.* **122** 171101